BIOCHEMISTRY
including biophysical chemistry & molecular biology
Article

*Biochemistry* **2010,** *49,* 1425–1434 1425
DOI: 10.1021/bi901565k

# Kinase-active Signaling Complexes of Bacterial Chemoreceptors Do Not Contain Proposed Receptor−Receptor Contacts Observed in Crystal Structures†

Daniel J. Fowler, Robert M. Weis, and Lynmarie K. Thompson*

*Department of Chemistry, 710 North Pleasant Street, University of Massachusetts, Amherst, Massachusetts 01003*

*Received September 8, 2009; Revised Manuscript Received December 11, 2009*

ABSTRACT: The receptor dimers that mediate bacterial chemotaxis form high-order signaling complexes with CheW and the kinase CheA. From the packing arrangement in two crystal structures of different receptor cytoplasmic fragments, two different models have been proposed for receptor signaling arrays: the trimers-of-dimers and hedgerow models. Here we identified an interdimer distance that differs substantially in the two models, labeled the atoms defining this distance through isotopic enrichment, and measured it with $^{19}F-^{13}C$ REDOR. This was done in two types of receptor samples: isolated bacterial membranes containing overexpressed, intact receptor and soluble receptor fragments reconstituted into kinase-active signaling complexes. In both cases, the distance found was not compatible with the receptor dimer−dimer contacts observed in the trimers-of-dimers or in the hedgerow models. Comparisons of simulated and observed REDOR dephasing were used to deduce a closest approach distance at this interface, which provides a constraint for the possible arrangements of receptor assemblies.

The bacterial chemotaxis system offers a unique opportunity to study transmembrane signaling in structural and mechanistic detail (*1*). As bacteria swim through their environment, they execute a random walk consisting of runs and tumbles that biases the motion toward higher concentrations of chemical attractants, including nutrients like serine, and away from repellants, such as toxic substances like $Ni^{2+}$. The proteins that control chemotactic behavior and the underlying signaling logic have been identified; these are summarized in Figure 1. Transmembrane chemoreceptors together with the scaffolding protein CheW and the signaling kinase CheA form signaling complexes that are found predominantly in clusters at the cell poles. Phosphotransfer from CheA to CheY elicits tumbling upon binding of CheY-phosphate to switch proteins in the flagellar motor. Tumbling is suppressed by attractant binding to the chemoreceptor, which inhibits CheA activity thereby lowering levels of CheY-phosphate. Adaptation to ambient chemoeffector concentrations is mediated by the enzymes CheR and CheB, which modulate the receptor sensitivity by adding and removing methyl groups to four specific residues on the chemoreceptor. These methyl transfer reactions take place on a slower time scale than attractant-mediated kinase inhibition and stimulation, so the methylation state becomes a memory of the conditions the cell experienced several seconds prior. Consequently, cells respond to gradients of attractants and repellents.

Despite the challenges of understanding the structure and interactions of a multiprotein, membrane-bound complex, a good deal of progress has been made by employing two divergent strategies. At relatively low resolution fluorescence (*2*), electron microscopy (*3*−*11*) and site-directed cysteine cross-linking (*12*−*15*) have been used to probe the cellular localization and arrangement of proteins within signaling complexes. High-resolution structures of all the proteins in the signaling pathway have been determined for individual proteins, or in the case of the receptor as separated (soluble) periplasmic and cytoplasmic domains.

The detailed arrangement of proteins in signaling assemblies comprised of chemoreceptors, CheA, and CheW is not known. Models for the intact receptor have been deduced from structures of various fragments corresponding to much of the receptor sequence, including crystal structures of the periplasmic (*16*) and cytoplasmic (*17*) domains, and an NMR structure of the HAMP domain that connects the transmembrane and cytoplasmic domains (*18*). Models for receptor−receptor packing in extended signaling arrays have been proposed based on packing interactions observed in crystals of cytoplasmic domains. The structures of cytoplasmic domains of the *Escherichia coli* serine receptor (*17*), a *Thermotoga maritima* chemoreceptor of undetermined ligand specificity (*19*), and a putatively cytosolic receptor, also from *T. maritima* (*20*), are all extended four-helix bundles that are comprised as homodimers of coiled-coil hairpins. However, the structures differ in how these bundles pack together in the crystal (Figure 2). The *T. maritima* dimers pack close together in a linear array or "hedgerow". The *E. coli* domains are packed as a trimer of dimers: three dimers with 3-fold rotational symmetry contact one another at the cytoplasmic tip but splay apart in the region that corresponds to the membrane-proximal end. These two packing arrangements have been used to generate two different array models of the receptor/CheW/CheA signaling complex. Crane and co-workers proposed the hedgerow model based on the dimer−dimer packing observed in the *T. maritima* crystals, which were assembled into an extended array with data from the structures of CheW and CheA domains (*19*). Independently, Bray and colleagues, and later Kim and colleagues, have

†This research was supported by U.S. Public Health Service Grants GM47601 to L.K.T. and GM53210 to R.M.W. D.J.F. was partially supported by National Research Service Award T32 GM08515 from the National Institutes of Health. The University of Massachusetts Mass Spectrometry Facility receives partial support from the National Science Foundation.

*To whom correspondence should be addressed. E-mail: thompson@chem.umass.edu. Phone: (413) 545-0827. Fax: (413) 545-4490.


Published on Web 01/20/2010

proposed a model with hexagonal symmetry, the trimers-of-dimers model, based on the packing observed in the crystals of the *E. coli* serine receptor cytoplasmic domain (*21*, *22*). In a recent paper, Jensen and co-workers have reported that hexagonal packing of chemoreceptor arrays is widespread among a variety of bacteria including *T. maritima* (*23*), which argues against the hedgerow organization observed in crystals of *T. maritima* receptor fragments. Although the hexagonally averaged electron density maps generated by cryoelectron microscopic tomography of chemoreceptors and signaling proteins in cells have sufficient resolution to fit receptor subunits, the resolution is insufficient to identify the arrangement of proteins in the complexes in atomic detail (*4*−*6*).

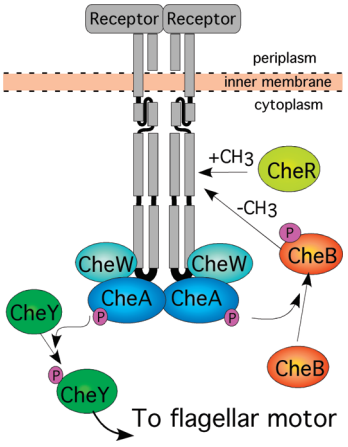


FIGURE 1: The chemotaxis signaling system. The transmembrane receptor dimer interacts with cytoplasmic proteins, which together form a signaling circuit that couples changes in external ligand concentrations to chemotactic swimming behavior.

Here, we have performed a direct structural measurement using site-directed solid-state NMR to probe the nature of dimer−dimer contacts within a more native context than crystals of receptor fragments. This method enjoys the angstrom-level resolution of crystallography but allows us to examine these contacts in the context of the intact, membrane-bound receptor and a cytoplasmic domain/CheW/CheA complex, without the need for obtaining diffracting crystals whose assembly may depend on the formation of non-native protein−protein contacts. The site-directed nature of the experiment also allows us to probe multiprotein complexes that are too large for uniformly labeled solid-state NMR experiments (due to spectral overlap) and far too large for solution NMR (due to slow correlation times). We analyzed the two models for receptor arrays for dimer-to-dimer distances that were distinctly different between the two and happened also to fall within the measurable range of the NMR method (~12 Å or less). From these we selected a pair of atoms amenable to isotopic labeling, prepared the relevant proteins, and measured the distance between the atom pairs in two types of samples: the intact chemoreceptor embedded in native membrane vesicles and the receptor cytoplasmic domain in functional complexes with CheA and CheW. As demonstrated below, a single key distance measurement provides an important test of structural models to aid in understanding the mechanism of signaling by this receptor.

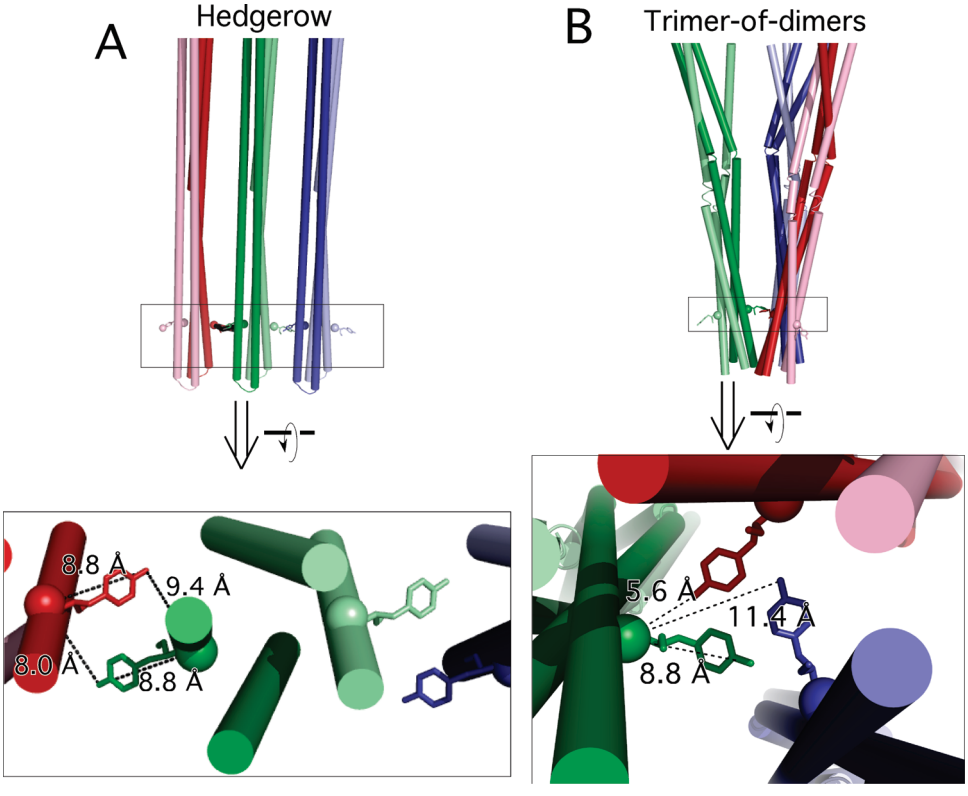


FIGURE 2: Different arrangements are proposed for receptor−receptor packing in signaling complexes. (A) Top: In the hedgerow model, receptor dimers pack in a linear array. Bottom: The view from the cytoplasm, looking toward the membrane. The modeled *p*-F-Phe residues are shown as sticks; labeled carbons are shown as spheres. Important C−F distances are labeled. (B) Top: In the trimers-of-dimers model, the receptor dimers touch at their cytoplasmic tips. Bottom: The trimer of dimers as viewed from the cytoplasm. 3-fold symmetry is present, but each type of distance is labeled only once, for clarity. Not shown are the monomers not featured in the trimer contacts; each of these can be modeled as an isolated $^{13}C-^{19}F$ pair with an 8.8 Å distance (see Materials and Methods).

## MATERIALS AND METHODS

*Plasmids and Strains*. The serine receptor and the cytoplasmic fragment (CF)[1] of the aspartate receptor used in this study contained glutamine residues at the four major sites of methylation; glutamine substitution at the methylation sites is known to mimic the effects of receptor methylation (*24*). The plasmid pJL31.A372C was constructed from pJL21 (*25*) to encode the fully modified (4Q) *E. coli* serine receptor with a 34 residue truncation from the C-terminus, a 6×His affinity tag fused to the truncated C-terminus and the A372C substitution. The plasmid pHTCF.4Q encodes the N-terminally His-tagged, fully modified aspartate receptor cytoplasmic fragment and ampicillin resistance (*26*). pHTCF.4Q.A372C containing the A372C mutation was made using a QuikChange site-directed mutagenesis kit (Stratagene). Residue numbers in all proteins studied are expressed in terms of the corresponding residue number in the intact serine receptor to allow direct comparison to the pdb entry 1qu7. pCF430 carries tetracycline resistance as well as a *lacI*$^q$ and was provided by Steve Sandler (Department of Microbiology, University of Massachusetts Amherst). The *E. coli* strain DL39C is auxotrophic for multiple amino acids, including Phe and Cys, which promotes efficient incorporation of NMR labels. The Cys auxotrophy is due to the insertion of a transposon into the *cysE* gene and is maintained with kanamycin selection (*27*). DL39C was transformed with pHTCF.4Q.A372C and pCF430 to generate reproducible high-level CF expression after induction by IPTG.

*Protein Expression and Purification*. CheA was purified as in the published procedure (*28*), but ion-exchange chromatography was omitted. CheY was purified as previously published (*29*). CheW was purified as published (*30*) but with an added size-exclusion chromatography purification: pooled fractions from the ion-exchange column were concentrated with 10 kDa concentrators (Amicon) and loaded in 3 mL aliquots to a preequilibrated column (HiPrep 26/60 Sephacryl S-100 HR; GE Healthcare); the column was run at 1 mL/min with PIP buffer (10 mM piperazine, 100 mM NaCl, 0.5 mM EDTA, pH 6.0) (*30*), and CheW fractions were pooled, concentrated, and frozen in aliquots.

Isotopically enriched serine receptors in inner membrane vesicles were expressed from DL39C/pJL31.A372C. Different defined media were used for growth and expression, as reported previously (*27*), with the minor modification that racemic *p*-F-Phe (at twice the concentration) was used in place of the L-enantiomer. Inner membranes containing the overexpressed receptors were isolated, also as previously described (*31*). To perform the natural abundance $^{13}C$ correction required for REDOR experiments (*27*), two types of receptors were prepared: labeled receptors with $^{13}C$-enriched cysteine and unlabeled receptors with $^{13}C$ present in natural abundance. All serine receptors incorporated *p*-F-phenylalanine in place of Phe.

Fully modified CF ($CF_{4Q}$) was expressed from DH5α/pHTCF.4Q. Cells were grown in LB with ampicillin (150 μg/mL) to an optical density of 0.4−0.6, at which point IPTG was added to 500 μM and protein expression continued for 3 h.

$CF_{4Q}$ A372C was expressed from DL39C/pHTCF.4Q.A372C/pCF430. Cells were grown to an optical density of 1.0 in LB with ampicillin (150 μg/mL), kanamycin (50 μg/mL), and tetracycline (50 μg/mL). Cells were then pelleted, washed, and resuspended in expression media, which contained ampicillin but not kanamycin or tetracycline (*27*). IPTG was added to the cells to 500 μM, and protein was expressed for 3 h. As with the serine receptors, both labeled and unlabeled CFs were prepared.

All CFs were purified on HisTrap columns (GE Healthcare) (buffer conditions: 75 mM $K_xH_{3-x}PO_4$, pH 7.5; imidazole 15 mM loading, 50 mM wash, 500 mM elution; buffers for cysteine mutants contained 2 mM TCEP). CF purity was good, as judged by SDS−PAGE, but isolated CFs consistently contained a proteolysis product running at a slightly lower molecular weight; mass spectrometry indicates the fragment is ∼1900 Da (∼16 residues) smaller than the intact CF. The proteolysis probably removed the His-tagged N terminus, because the proteolyzed CF did not cosediment with the templating lipid vesicles. Activity assays were performed under conditions that corrected for this, by equating the sedimenting fraction of CF: the total CF concentration in PEG-containing assemblies was set equal to the intact CF concentration in lipid-mediated assemblies.

*Fluorine Incorporation*. Levels of *p*-F-phenylalanine incorporation in both intact Ser receptor and Asp receptor CFs were estimated by trypsinolysis and mass spectrometry. Proteomics-grade trypsin (Sigma) was dissolved in $ddH_2O$ (0.2 mg/mL) on the day of use. Samples containing 75 μg of CF, 5 μg of trypsin, and 19 mM $NH_4HCO_3$ (50 uL total volume) were incubated overnight at 37 °C. Samples were processed the next day with PepClean C18 columns (Pierce) according to the directions. Peptides were eluted in 70% acetonitrile and subjected to MALDI-MS analysis.

The CF sequence contains four Phe residues, predicted to reside in four different peptides upon trypsin digest (predicted masses 992, 1349, 1004, and 2914 Da). For each of these peptides a +18 Da peak was detected, indicating successful *p*-F-Phe incorporation. In some but not all cases a very low signal-to-noise peak could be detected at the *m*/*z* ratio corresponding to the unsubstituted peptide; the overall incorporation rate was therefore taken to be ∼100%. Trypsin-digested intact serine receptor gave more complex, lower signal-to-noise spectra. Based on the high level of protein overexpression, and the choice of the same Phe-auxotrophic strain used for CF expression, full *p*-F-Phe incorporation was not problematic. The one observed peak identified as being diagnostic of $^{19}F$ incorporation (1577 to 1595 *m*/*z*, corresponding to residues 35−47) showed a pronounced shift to the +18 *m*/*z* ratio, although poor signal-to-noise ratio precluded accurate quantitation. Complete $^{19}F$ incorporation was therefore assumed as in the CF samples.

*Kinase Assays*. CheA, CheW, and CF (plus lipid vesicles and/or PEG buffer) were incubated overnight at 25 °C to allow full assembly of complexes. In samples containing vesicles, the membranes were comprised of DOPC and DOGS-NTA-$Ni^{2+}$ in a 1:1 molar ratio. Vesicles were prepared by extrusion 15 times through a track-etched polycarbonate membrane with 50 nm diameter pores (Avanti Polar Lipids, Alabaster, AL) as described previously (*30*). Kinase assays were conducted using the enzyme-coupled method as described previously (*32*).

[1]Abbreviations: CF, cytoplasmic fragment of Asp receptor; DMSO, dimethyl sulfoxide; DOGS-NTA, 1,2-dioleoyl-*sn*-glycero-3-[(*N*-(5-amino-1-carboxypentyl)iminodiacetic acid)succinyl; DOPC, 1,2-dioleoyl-*sn*-glycero-3-phosphocholine; EDTA, ethylenediaminetetraacetic acid; HAMP, histidine kinases, adenylyl cyclases, methyl binding proteins and phosphatases; IPTG, isopropyl β-D-1-thiogalactopyranoside; LB, Luria−Bertani broth; PDB, Protein Data Bank; PEG, polyethylene glycol; REDOR, rotational echo double resonance; SDS−PAGE, sodium dodecyl sulfate−polyacrylamide gel electrophoresis; TCEP, tris(2-carboxyethyl)phosphine.

To mimic the slow freezing experienced by samples prior to a REDOR experiment, the following protocol was used. Samples were assembled, and an aliquot was removed and assayed for initial activity. The sample was pelleted at 139000*g* for 15 min in a small centrifuge tube. The supernatant was pipetted away, frozen in liquid nitrogen, and stored at −80 °C. The centrifuge tube containing the pellet was sealed with parafilm, closed in an Eppendorf tube, and immersed in a room temperature ethylene glycol/water bath, which was then placed in a −80 °C freezer overnight. A small aliquot of the supernatant was thawed by immersion in a 25 °C water bath and then checked for activity (typically yielding no kinase activity). The centrifuge tube containing the pellet was then immersed briefly in the water bath (until visibly thawed). The whole of the supernatant was added back to the pellet and resuspended with brief, vigorous pipetting; kinase activity was measured immediately afterward.

Proteins assembled on DOPC/DOGS-NTA-$Ni^{2+}$ vesicles in buffers comparable to those previously used (75 mM Tris, 5% DMSO, 50 mM KCl, 25 mM $MgCl_2$, and 2 mM TCEP) (*26*) retained only ∼50% activity after the freeze−thaw treatment. Modest improvements were obtained by switching from Tris to potassium phosphate buffers, presumably due to the much smaller temperature change in p$K_a$ that phosphate buffers experience relative to Tris (*33*). This is likely to be broadly applicable to solid-state NMR experiments that are performed at temperatures lower than that at which the sample is prepared. However, we note that the use of potassium rather than sodium phosphate is important, as others have shown that sodium phosphate buffers can undergo radical pH shifts upon freezing. (*34*) Although the DMSO in the original buffer reduced the slow-freeze damage, it was incompatible with our solid-state NMR experiments, as DMSO forms very low freezing point mixtures with water. At the minimum temperature readily maintained in our NMR probe (nominally 213 K), a portion of the sample remained liquid when DMSO was present, which greatly increased the propensity of the sample to heat under the applied radiofrequency irradiation (data not shown). The PEG/trahalose mixture that was found to prevent slow-freeze damage also did not promote RF-induced heating in the NMR experiment.

*Model Construction*. Trimer-of-dimers and hedgerow structures containing *p*-fluorophenylalanine were constructed in Pymol from the published PDB files 1qu7 and 2ch7, respectively (*17*, *19*). In both cases, symmetry mates were generated first. For the hedgerow structure, a phenylalanine had to be substituted into the *T. maritima* structure, because the *T. maritima* contained another amino acid at this position. Alignment of the *T. maritima* and *E. coli* sequences was performed (http://www.ebi.ac.uk/Tools/emboss/align/index.html), and the residue in the *T. maritima* sequence (E358) corresponding to F373 in the *E. coli* serine receptor was identified. E358 residue was mutated to phenylalanine and an appropriate rotamer selected from Pymol's backbone-dependent library. Among the several rotamers available, only the rotamer shown in Figure 2 is consistent with our final REDOR results. The others necessarily give $^{13}C-^{19}F$ distances shorter than 8.8 Å, due to intramonomer interactions, and so these are not considered further here. Hydrogen atoms were then added to both structures using Pymol h_add function and fluorine substitutions made at the para position.

*REDOR NMR and Analysis*. All NMR experiments were performed on a 300 MHz Infinity+ spectrometer (Varian) equipped with an XR sample cooler from FTS Systems. The $^{19}F$ dephasing pulse widths were chosen by optimizing the REDOR dephasing, using a fluorinated inclusion compound designed for that purpose. We have since shown that after such an optimization is used, we observe correct REDOR dephasing for at least 64 rotor cycles (Fowler and Thompson, unpublished results). Performance of the REDOR experiment was checked against fluorinated polycarbonate immediately before acquiring data on the intact Ser receptor, and both before and after acquiring data on the CF-CheA-CheW complex. In all three cases the polycarbonate REDOR data fit to dipolar coupling values of 1900−2000 Hz, consistent with published results (*35*). REDOR on intact Ser receptor was performed with 40960 $S$ and $S_0$ scans per dephasing time per sample. Data were collected by cycling through three dephasing times (4.8, 8.0, and 11.2 ms). The pulse delay was 1 s, giving a total experiment time of 68 h for each (labeled and unlabeled) sample. Data were collected in blocks containing 1024 scans each $S$ and $S_0$; 1 scan of $S$ was followed by 1 scan of $S_0$ for a single dephasing time, until the block was completed, followed by a block of $S$ and $S_0$ scans for the next dephasing time. This process repeated until all scans were obtained. Power levels for $^{13}C$, $^{19}F$, and $^{1}H$ decoupling pulses were 50, 80, and 80 kHz, respectively. Cross-polarization was performed with a linear ramp. Proton decoupling was continuous wave. The spinning speed was 5 kHz and the nominal temperature (that of the cooling gas) was maintained at −50 °C. Data were oversampled (500 kHz sweep width) and decimated before processing. Line broadening was Lorentzian and match-filtered to the estimated width of the unbroadened, background-subtracted $S_0$ spectrum (438 Hz). FIDs were zero-filled once. Natural abundance contributions to the REDOR dephasing were removed as follows: $S$ and $S_0$ spectra were processed for both the $^{13}C$-labeled and the unlabeled spectra. An integral over the $S_0$ aliphatic region was taken for each, and the labeled spectra were scaled by the ratio of these integrals. Finally, the unlabeled $S$ and $S_0$ spectra were subtracted from the corresponding labeled spectra, yielding REDOR spectra free from natural abundance $^{13}C$. Peak intensities of the carbonyl peaks were used to calculate the quantity $((S_0 - S)/S_0)$.

REDOR spectra of the Asp receptor CF complexes were collected and processed as for the Ser receptors, with the following exceptions. 46080 $S$ and $S_0$ scans were collected per dephasing time per sample, in blocks of 512. Pulse delay was set to 1.5 s. Some blocks contained excessive amounts of noise, for reasons poorly understood; these blocks were readily identified and were discarded prior to summation of the remaining blocks. Decoupling was TPPM. Line broadening was 126 Hz, derived using the match-filtered condition described for the intact Ser receptor. The temperature of the cooling gas was maintained at −60 °C; in-house calibration indicates this corresponds to an actual sample temperature of −40 °C.

Uncertainties in all measurements were estimated using the rms of the baseline. For experiments on the intact receptor, peak intensities were measured as peak heights with uncertainties equal to the rms of the baseline. For experiments on the CF complexes, peak intensities were measured as peak integrals with uncertainties equal to the rms of the baseline times the square root of the number of points in the integration. Uncertainties in $\Delta S/S_0$ were calculated by error propagation to yield the error bars shown in Figure 3. CF spectra are shown in Figure S1 and intensities are tabulated in Table S1 in the Supporting Information.

REDOR dephasing times were initially chosen based on the expected curve for the trimers-of-dimers model, which predicted maximal dephasing by 10 ms (as shown in Figure 3). The benefit

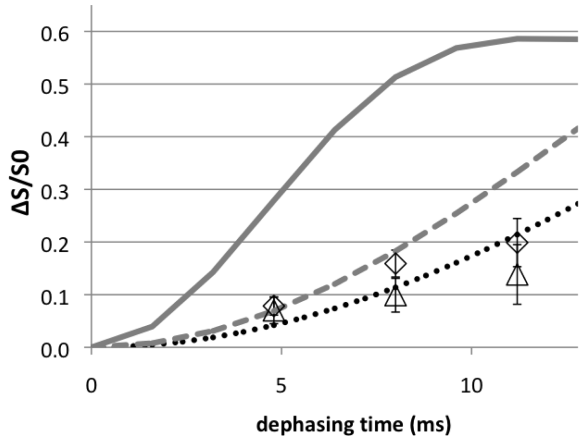


FIGURE 3: Predicted and observed REDOR dephasing. Curves are simulations for proposed receptor array structures: trimer of dimers (solid, gray), hedgerow (dashed, gray), and isolated dimers (dotted, black). Experimental data are shown for the intact serine receptor (diamonds), as well as a cytoplasmic fragment of the aspartate receptor in PEG-promoted active signaling complexes (triangles). Error bars were computed as described in Materials and Methods. Spectra and tabulated data for the active complexes are provided as Supporting Information.

of extending the experiment out to longer dephasing times was estimated with the trade-off between the signal loss due to relaxation ($T_2^*$ = 6.68 ms for the Cys carbonyl, based on the $S_0$ intensities measured in the difference spectra) and the predicted dephasing for the longer 8.8 Å distance. We did not pursue longer dephasing times, because the predicted ratio of $\Delta S/S_0$ signal vs noise was maximal by 11.2 ms.

SIMMOL was used to translate PDB files into SIMPSON input files (*36*). All REDOR curves were simulated using SIMPSON (*37*). REDOR curves for the trimers-of-dimers structures were calculated in two parts: one for the three monomers with F373 pointing inward and one for the three monomers in which F373 points outward. The final curve is an equally weighted average of the two. For modeling PDB-derived structures, all dipolar couplings were considered. In the three-spin simulation depicted in Figure 6, $^{19}$F homonuclear couplings were omitted to ease automation of the calculations. These homonuclear couplings should not interfere with the REDOR calculation. A smaller subset of control simulations (not shown) indicated that with 5 kHz MAS, the fluorine homonuclear couplings had to exceed 5.7 kHz before they led to significant perturbations of the REDOR curve; such high couplings cannot be produced by fluorine nuclei that do not approach closer than the sum of their van der Waals radii.

## RESULTS

*REDOR Distance Measurements Can Distinguish between Two Models Proposed for Receptor Arrays*. The strategy in designing the site-directed solid-state NMR experiments is to find pairwise interactions that are characteristic of a given model and also readily labeled to create an isolated pair of spin $^1/_2$ nuclei. In this case we took advantage of a key phenylalanine residue in the *E. coli* aspartate and serine receptors that is positioned at the receptor dimer−dimer interface in both structural models (Figure 2), as well as a unique, nonperturbing Cys that can be introduced by mutagenesis at residue 372. These residues are chosen because Phe can be labeled with $^{19}$F, which enables longer distance measurements, and the Cys can be labeled uniquely with $^{13}$C, because the wild-type receptor lacks Cys. The selection of a nonperturbing Cys mutation in this system is aided by the existence of a large body of literature about Cys mutations and their effects on activity (*12*, *38*, *39*). Labeled proteins are prepared by expression in media containing *p*-F-Phe and 1-$^{13}$C-Cys. We then used a REDOR experiment to measure the distance between the two labels. This technique is a well-established tool in structural biology and can measure distances with a resolution that rivals X-ray crystallography (*40*). The shortest interdimer distance between $^{13}$C- and $^{19}$F-containing residues is remarkably short in the trimers-of-dimers structure (5.6 Å; see Figure 2B) and substantially longer in the hedgerow structure (8.0 Å). In both cases the interdimer distances are shorter than the shortest likely $^{13}$C to $^{19}$F distance within a dimer (8.8 Å in 1qu7), so the REDOR dephasing will be dominated by the interdimer interaction.

*REDOR of Overexpressed Intact, Membrane-Bound Ser Receptors Measures a Predicted Long Distance*. Although inner membrane vesicle preparations such as these NMR samples have been widely studied and shown to be functional in complex formation (*31*), ligand binding, (*41*) kinase (*39*, *42*), and methylation assays (*43*, *44*), recent studies have demonstrated that expression of chemoreceptors without sufficient amounts of CheA and CheW leads to an alternate receptor array structure that correlates with impaired chemotaxis (*7*). In this alternate structure the cytoplasmic tips of the receptor array are interdigitated with receptors from another array, which would disrupt the receptor dimer−dimer interactions observed in the trimers-of-dimers or hedgerow crystals. Given the high overexpression levels of intact receptor in our samples, without any overexpression of CheA and CheW, it is likely that the receptors are predominantly interdigitated. In such samples we do not expect REDOR dephasing due to dimer−dimer interactions but only due to fluorines within the same dimer. The closest carbon fluorine distance within the receptor monomer (or dimer), assuming the most probable rotamer in this α-helical context, is predicted to be 8.8 Å.

REDOR experiments were performed on a matched pair of samples of Ser receptors bound to native inner membrane vesicles. REDOR dephasing in the experimental sample (labeled with both 1-$^{13}$C-Cys and *p*-$^{19}$F-Phe) is the sum of the dephasing of $^{13}$C-Cys372 by *p*-$^{19}$F-Phe373 and the dephasing of natural abundance $^{13}$C by all of the *p*-$^{19}$F-Phe. The latter is removed by subtraction of the dephasing observed in the control sample (labeled with only *p*-$^{19}$F-Phe.) The resulting REDOR dephasing data in Figure 3 (diamonds) are consistent with the predicted curve for isolated dimers: the data fit well to a single distance of 8.8 Å (dotted line). This suggests that we have accurately measured a long distance, corrected for the natural abundance $^{13}$C contribution, in this complex sample.

*Kinase Assays Identify Conditions for NMR of Active Assemblies*. Biochemical assays that use kinase activity to interrogate receptor function, such as receptor-mediated kinase inhibition, assess only those receptors in communication with the kinase. However, the REDOR experiment measures dephasing in all the receptors in the sample, and therefore it is important to maximize the fraction of receptors in active complexes. By assembling complexes with the receptor cytoplasmic fragment (CF), we avoided the accessibility issues that can plague samples of intact receptors in membrane vesicles. We discovered new NMR-compatible conditions for assembly of CF/CheW/CheA signaling complexes, which we demonstrated to have a kinase

activity comparable to the activity observed with biochemically well-characterized complexes assembled on liposomes (*26*).

(*A*) *PEG/Trehalose Mixtures Suitable for NMR Also Promote Complex Assembly*. NMR of active samples requires buffer conditions that protect against damage during freezing (relatively slowly) and during high-power radio-frequency pulsing. A slow freeze−thaw protocol in the presence of cryoprotectants (see Materials and Methods) was followed by a measurement of kinase activity to determine the extent of damage to the sample. We tested a number of cryoprotectants and found that a combination of PEG 8000 (7.5% w/v) and trehalose (4% w/v) worked well to preserve activity of liposome-mediated complexes of CF, CheA, and CheW (Figure 4). We subsequently found that the PEG/trehalose conditions were sufficient to promote assembly of active complexes without the liposomes, suggesting that PEG (a known macromolecular crowding agent) drives the assembly of the large, sedimenting complexes. Inclusion of PEG/trehalose in the samples, with or without lipids, drove more CF and CheA into the sedimenting complexes, as judged by SDS−PAGE of pellets. Since the kinase activities of PEG-promoted complexes were similar to the activities of complexes formed on vesicles with comparable amounts of CF (Figure 4 and ref *30*), we concluded that the addition of PEG provides another effective means of assembling kinase-active signaling complexes. This is consistent with published accounts that soluble CFs can complex CheA and CheW in solution to form active complexes, if the right buffer conditions are used: Wolanin et al. found several such conditions (*10*), and Montefusco et al. have observed similar complexes via electron microscopy (*30*). It is also consistent with literature suggesting that PEG may be used to precipitate proteins while maintaining their structure and functionality (*45*, *46*). An alternate explanation, that PEG-induced precipitation increases CheA kinase activity independent of its incorporation in signaling complex, was ruled out with control samples in which either CF or CheW was omitted from the complexation reaction. These samples did not have detectable kinase activity under assay conditions (data not shown). We considered this finding fortuitous, because the vesicles have disadvantages for NMR; i.e., they occupy volume and may contribute paramagnetic line broadening. We therefore performed the REDOR experiments on PEG-promoted assemblies, samples assembled solely through the actions of PEG and trehalose with no liposomes present.

(*B*) *Receptor-Saturating Concentrations of Binding Partners Identified*. To maximize NMR sample homogeneity, we sought to drive as much as possible of the receptor fragment into active CF/CheW/CheA complexes. Since the activity of CheA increases 200-fold upon binding to receptors and CheW (*32*), we could easily use the kinase activity as the means to optimize the sample composition. We began by assembling complexes with a single CheA concentration (6 $\mu$M) and varied the CheW concentration from 0 to 50 $\mu$M. Under these conditions a maximum in activity was observed in samples containing 20 $\mu$M CheW (Figure 5A). We then prepared samples with 49 $\mu$M CF, 20 $\mu$M CheW, and various CheA concentrations, and a maximum in activity was observed at 12 $\mu$M CheA (Figure 5B). The sample formed under conditions that produced the largest activity, 49 $\mu$M CF, 12 $\mu$M CheA, and 20 $\mu$M CheW, was assumed to consist of complexes in which all the available binding sites on the CF were saturated with CheA and/or CheW. Although these concentrations were arrived at with samples that contained *both* vesicles *and* PEG and trehalose, comparable activities were observed when the vesicles were omitted. Vesicles were omitted for all NMR experiments on functional complexes.

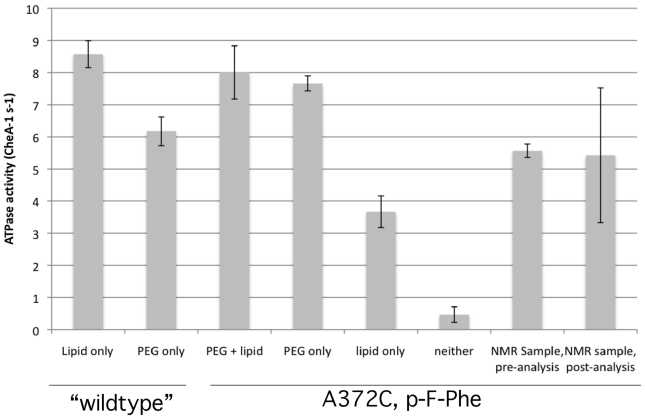


FIGURE 4: ATPase activity of CF/CheW/CheA signaling complexes. All activities are reported in terms of total CheA added. Samples at right are 4Q A372C mutants (in Tsr residue numbering) and have *p*-F-Phe at all Phe sites. "Wildtype" refers to samples with $CF_{4Q}$ that do not contain the A372C mutation and do not contain *p*-F-Phe. PEG samples contain 7.5% (w/w) PEG 8000 and 4% (w/w) trehalose. Lipid samples contain 1:1 DOPC:DOGS-NTA-$Ni^{2+}$ lipid vesicles at a total lipid concentration of 540 $\mu$M. The data show that PEG assembly yields active complexes and that both NMR labeling and NMR analysis are minimally perturbing to signaling complex activity. Error bars represent the standard deviation of at least two trials.

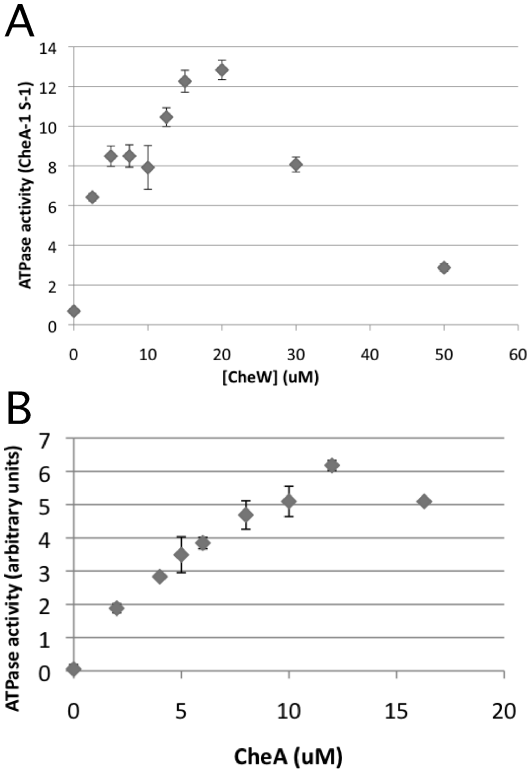


FIGURE 5: Conditions for maximal formation of kinase-active signaling complexes. (A) ATPase activity as a function of [CheW], using fixed [CheA] (6 $\mu$M) and [CF] (49 $\mu$M). Maximal activity is seen at 20 $\mu$M CheW. (B) ATPase activity as a function of [CheA], using fixed [CheW] (20 $\mu$M) and [CF] (49 $\mu$M). Error bars represent the standard deviation of at least two trials. Samples are PEG-promoted assemblies but also contain liposomes.

(*C*) *NMR Labeling Is Minimally Perturbing*. The A372C mutation is similar to one used previously, which did not to disrupt receptor function (*38*), so A372C was not expected to

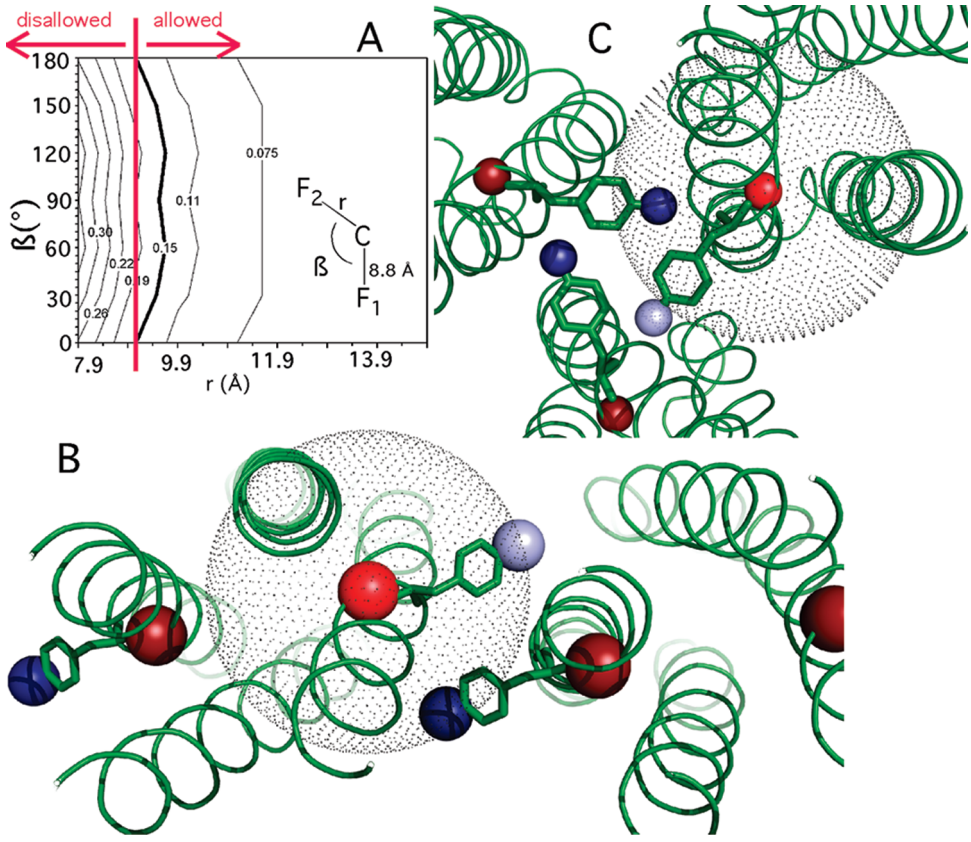


FIGURE 6: Closest approach limits of a second dimer. (A) Calculated difference between predicted and observed REDOR dephasing of the carbon as a second fluorine (F2) approaches at a distance $r$ and angle $\beta$. (B) Close-up view of the hedgerow model, illustrating the impact of the REDOR constraint. The selected carbon at the center of the sphere (bright red) is dephased by the fluorine from the same monomer (light blue); the dotted 8.8 Å sphere should exclude the other fluorines, but one (dark blue) intrudes. (C) The closest REDOR-allowed approach in the trimers-of-dimers model of a different monomer's fluorine is 7.9 Å (see text), but the model shows a dark blue fluorine approaching closer.

disrupt function either. However, substitution of phenylalanine with fluorophenylalanine at all positions can disrupt protein function, and so the combined effects of the cysteine mutation and fluorophenylaline incorporation on kinase activity were measured. The combination was shown to be nonperturbing under PEG/trehalose assembly conditions (Figure 4). The wild-type CF, unlike the mutant/F-labeled receptor, yielded a greater activity in complexes assembled with lipid vesicles than CF/CheW/CheA samples induced to assemble with PEG; we know too little about the assembled complex to speculate about the origin of this difference.

*REDOR Demonstrates Receptor Packing in Active Arrays Differs from Both Crystals*. REDOR experiments were performed on PEG-promoted assemblies of the CF (A372C, 4Q), CheA, and CheW, labeled with either 1-$^{13}$C-Cys and *p*-$^{19}$F-Phe or only *p*-$^{19}$F-Phe. The natural abundance contribution to dephasing, measured on the sample labeled only with p-$^{19}$F-Phe, was subtracted from the dephasing of the 1-$^{13}$C-Cys and *p*-$^{19}$F-Phe labeled sample. Peak integrals were measured in NMR difference spectra (Supporting Information Figure S1) for $S$ and $S_0$ at each dephasing time. These were used to calculate $\Delta S/S_0$ data (Supporting Information Table 1), which are plotted in Figure 3 (triangles). The REDOR dephasing data are clearly incompatible with the interdimer packing interactions of both the trimers-of-dimers and the hedgerow crystal structures. Instead, the result once again fits well to a single distance of 8.8 Å. This is the distance observed in the trimers-of-dimers crystal structure to separate the introduced $^{19}$F and $^{13}$C labels within a single monomer of the receptor. It also the greatest possible separation of the labels in a single monomer, assuming that Phe373 adopts an "allowed" rotamer and that the receptor retains its α-helical character.

The actual sample used in the REDOR experiment was assayed for kinase activity before and after the experiment (Figure 4). The sample was difficult to resuspend uniformly following NMR analysis, which resulted in larger variation in activity among sample aliquots. Nonetheless, full activity was observed in the post-NMR sample (Figure 4), which is the average activity measured on five aliquots taken from this sample.

The PEG-promoted CF/CheA/CheW assemblies are substantially more homogeneous than the intact-receptor vesicle samples as judged by NMR line widths. The 1.7 ppm line width of the unique Cys carbonyl carbon, i.e., labeled minus unlabeled spectrum, of the active assemblies compares favorably with the 1.5−3.0 ppm range observed for well-folded, noncrystalline proteins (*47*−*50*).

The REDOR results indicate that in the active signaling complex, receptors do not approach one another as closely at this interface as they do in the crystal structures. To further clarify how closely together the receptors in the complex might approach one another, without contradicting the NMR measurement, we conducted a series of simulations with the SIMPSON NMR package (*37*). REDOR dephasing of a single $^{13}$C atom was simulated with a single $^{19}$F atom (representing Phe373 from the same monomer) fixed at a distance of 8.8 Å. A second $^{19}$F was then introduced, and its influence on dephasing was investigated as a function of its distance from the carbon atom and the angle between the two carbon−fluorine dipole vectors, as depicted in Figure 6A. A REDOR curve was simulated for each arrangement, and the difference between the simulated and experimental

values was calculated for the most diagnostic, i.e., 11 ms, time point. The difference is plotted as a function of the position (distance and angle) of the second fluorine atom (Figure 6A). The difference values ($\Delta S/S_{0,\text{simulation}} - \Delta S/S_{0,\text{experiment}}$) are depicted as contours. The bold contour differentiates values that deviate from the observed value by more or less than twice the standard deviation. Therefore, all values to the left of the magenta line differ by more than this amount and are regarded as inconsistent with experiment. Thus, we see that the fluorine in the fluorophenylalanine from a second dimer cannot approach closer than ~8.8 Å. The magnitude of the discrepancy is illustrated in Figure 6B, which depicts a 8.8 Å sphere around a single $^{13}$C-labeled backbone carbonyl carbon (bright red) in the hedgerow model. To be consistent with our NMR data, none of the (dark blue) fluorine labels from another dimer should be within this sphere. The fluorine colored light blue is in the same monomer, equivalent to the "F1" in Figure 6A, and by definition is not subject to constraints on the approach of a second dimer. For clarity only one 8.8 Å sphere is shown, although equivalent spheres surround the other (dark red) carbons as well.

The model discussed above assumes that both monomers of a dimer participate equally in higher order interactions. Such a model is appropriate for the hedgerow model, where each dimer is contacted on both sides by additional dimers. However, in the trimers-of-dimers model only one of the two monomers in the dimer have an inwardly pointing phenylalanine that contributes significantly to the dephasing through higher order interactions. To adjust for this situation where only one monomer participates in the packing interaction, we performed a modified version of the closest possible approach analysis described above. In this case, the results of the three-spin REDOR simulations were averaged with the predicted results for a single 8.8 Å distance; the resulting curves were then compared to the experimental data, as before, and the same criterion was applied for compatibility with experiment. The resulting volume of closest approach again had little angle dependence, i.e., was spherical (data not shown). However, the radius in this case was reduced to 7.9 Å. Figure 6C shows the trimers-of-dimers model with this 7.9 Å distance mapped around a single $^{13}$C label. Again, the model is seen to be incompatible with the REDOR results as fluorine from a neighboring dimer (dark blue) is found within the volume of closest approach.

## DISCUSSION

This REDOR experiment provides a direct high-resolution structural measurement probing the nature of receptor dimer−dimer interactions in overexpressed intact membrane-bound receptors and functional assemblies of the receptor cytoplasmic domain with CheA and CheW. In both types of samples the receptor tips are not packed with either the trimers-of-dimers contacts or hedgerow dimer contacts originally proposed based on crystal structures of receptor cytoplasmic fragments (*17*, *19*). Instead, both samples show REDOR dephasing consistent with a single C to F distance of 8.8 Å, predicted to be the shortest distance within a receptor monomer. This was the expected result for the overexpressed intact receptor, suggesting the REDOR distance measurement is accurate, but was unexpected for the functional complexes, suggesting that any trimeric arrangement adopted by receptor dimers arises from interactions other than those captured in the trimers-of-dimers crystal structure.

Although native inner membrane vesicles containing overexpressed intact receptors have been shown to be functional in ligand binding, methylation, kinase activation, and transmembrane signaling (*38*, *43*), electron microscopy studies have shown that receptors overexpressed in the absence of CheA and CheW form an interdigitated interaction (*5*, *11*), which correlates with reduced chemotactic swarming (*7*). In a sample comprised of interdigitated receptor dimers, the REDOR experiment is not expected to detect the shorter dimer−dimer distances that arise from the contacts observed in the crystal structures, but only the longer intradimer carbon−fluorine distance. Our measurement of the expected 8.8 Å intradimer distance in this sample suggests these NMR conditions can be used to successfully measure a long distance in a complex sample and sets the stage for REDOR experiments on functional PEG-promoted assemblies of the receptor cytoplasmic fragment, CheA, and CheW. Through careful biochemical characterization of these assemblies, we have maximized formation of kinase-functional complexes. Our NMR experiments clearly demonstrate that the cytoplasmic domain in kinase-active samples does not have the dimer−dimer contacts observed in either the trimers-of-dimers or hedgerow crystal structures.

Although there is compelling evidence that chemoreceptors from a wide variety of bacteria organize in arrays with hexagonal symmetry, which is plausibly explained by a trimers-of-dimers receptor organization, our results demonstrate that the particular packing arrangement seen in the trimers-of-dimers crystal is not present in a kinase-active signaling complex. If it were, the interdimer $^{13}$C−$^{19}$F distance would be 5.6 Å; instead, it is found to be ≥7.9 Å, or at least 2.3 Å (~40%) longer. The trimers-of-dimers interface observed in the crystals is too small to be likely to be a physiologically relevant protein−protein interface. For example, online analysis of the 1qu7 trimers-of-dimers coordinates by PQS (protein quaternary structure) or PISA (protein interfaces, surfaces, and assemblies) both suggest that it is simply dimeric: the two trimers-of-dimers contacts made by each dimer have interface areas of only 200−300 Å$^2$, which correspond to predicted values of $\Delta G$ for interface formation between −1.7 and −2.5 kcal/mol. These values are similar to those found in a separate, obviously nonphysiological dimer−dimer contact in the same crystal structure (431 Å$^2$ and −1.5 kcal/mol). Therefore, invoking even small distortions or dynamics in the structure, to make it consistent with the measured 7.9 Å sphere of closest approach, would disrupt completely this already small interface. Our data suggest that if receptors in functional arrays form trimers of dimers, they pack together in some other arrangement not present in the crystal due to the absence of binding partners and/or the rest of the receptor, either of which could lead to the formation of nonphysiological crystal packing interactions. For example, our data are consistent with the model of the signaling complex derived from the electron microscopic analysis of kinase-active CF/CheW/CheA complexes (*3*). Although the resolution was insufficient to determine subunit contacts, the electron density was consistent with a functional unit comprised of three receptor dimers held separate from each other by the bound CheA and CheW. The demonstrated functionality of the samples used in this electron microscopy study and in our REDOR study indicate that these structures capture the protein−protein interactions needed for kinase activity, even if they do not capture all of the organization that occurs in the cell.

In addition to the observed crystal packing, substantial biochemical evidence has been invoked in support of the trimers-of-dimers interaction. The Parkinson laboratory in particular has found a number of mutations near the cytoplasmic tip

that interfere with proper functioning of the receptor. When some of these mutations are introduced into one receptor, e.g., the serine receptor, they interfere with the function of neighboring receptors of different ligand specificity, i.e., the aspartate receptor (*51*, *52*). In other cases, a specific mutation made to the second (aspartate) receptor can restore function to the first or both. Although this clearly indicates some sort of coupling between the different types of receptors, almost none of the perturbing and rescuing residues are predicted to be in contact within the proposed trimers-of-dimers structure and some would lie 20 Å or more distant from one another (tar414-tsr377). Such results are compatible with arrangements of receptors dimers other than the trimers-of-dimers arrangement observed in the crystal structure: for example, models in which the receptor dimers do not contact one another directly and are functionally coupled through mutual interactions with CheA and CheW. Interestingly, a similar lesion and rescuing mutation study sought to determine the residues of the receptor that interacted with CheW (*53*) and implicated residues that map to essentially the same face as the residues in the Tar-Tsr study. Thus, it may be that both studies are probing the same underlying phenomenon: a physical association of a receptor with CheW, which then, via this interaction, couples to neighboring receptor dimers.

Cross-linking data are also often cited in support of the occurrence of the trimers-of-dimers structure in cells. Studdert and Parkinson treated cells expressing Cys mutant receptors with a trifunctional cross-linking agent predicted to have the right spacer length to react with all three cysteines in the trimers-of-dimers structure. They found that ~50% of receptors were cross-linked by the reagent, forming a mixture of trimers and dimers. These data are consistent with the trimers-of-dimers model packing observed in the crystal structure, but also, as the authors of the original work stated, with a variety of other arrangements that might bring receptors close together (*15*). While these cross-linking results and the observation of hexagonal packing are both compatible with an organization of receptor dimers as trimers, our data provide a high-resolution test indicating that such an organization of the kinase-active state does not occur via the interface observed in the crystal structure.

Although our data also do not support the originally proposed hedgerow arrangement of dimers (*19*), the distinction is not as clear as it is for the trimers-of-dimers crystal structure, because the measured distance (8.8 Å) is closer to the predicted distance (8.0 Å). Interestingly, a structure reported recently (*20*) for a soluble chemoreceptor (with a distorted structure within the dimer) also packs in hedgerows, but in a manner consistent with our NMR constraint: the dimers within a hedgerow are rotated about 90° from their position in the earlier hedgerow structure, such that the sites we probed would be quite far from the interface and the distance corresponding to our NMR measurement would be over 8.8 Å. The fact that a variety of dimer−dimer contacts are observed in the crystals, including three that seem physiologically plausible, but also others that are clearly not relevant, demonstrates the importance of devising a direct structural measurement to test any proposed array model. The REDOR experiment reported here provides just such a test, under conditions that capture (at a minimum) the structural determinants of CheA kinase activation.

Finally, this study is yet another example of how solid-state NMR can be used to obtain high-quality structural information in systems that are both extremely complex and biologically relevant. In studies of proteins as diverse as isomerases (*45*), peroxidases (*54*), and cytochrome oxidases (*46*), combining biochemical assays with structural techniques has been important to ensure that NMR analysis is being done on proteins in their functional state. Our study also demonstrates that by employing a highly focused, site-directed strategy to minimize spectral complexity, solid-state NMR can be used effectively to study a large multiprotein complex (multiple copies of the 33 kDa CF, 18 kDa CheW, and 71 kDa CheA) representing one signaling state of a transmembrane receptor array. This targeted strategy was sufficient to test and invalidate a specific structural hypothesis. The biochemical optimization of the system has yielded narrower line widths that make this complex amenable to some high-resolution techniques. Such approaches are increasingly being applied to systems of remarkable complexity, such as microtubule−dynactin complexes (*55*) and phospholamban−calcium ATPase complexes (*56*). Future solid-state NMR experiments, together with the wealth of structural data already available, are a promising approach for obtaining a detailed picture of the intact signaling complex.

## ACKNOWLEDGMENT

For helpful discussions about NMR spectroscopy we thank Jim Frye and Kevin Geohring. We thank Mona Gupta for construction of the pJL31.A372C plasmid, Stephen Eyles for assistance with mass spectroscopy, and Sandy Parkinson for helpful comments on the manuscript. Some figures were generated with PyMol.

## SUPPORTING INFORMATION AVAILABLE

NMR spectra (Figure S1) and $\Delta S/S_0$ tabulated data (Table S1) for receptor cytoplasmic fragments in kinase-active complexes with CheA and CheW. This material is available free of charge via the Internet at http://pubs.acs.org.

## REFERENCES

1. Wadhams, G. H., and Armitage, J. P. (2004) Making sense of it all: bacterial chemotaxis. *Nat. Rev. Mol. Cell. Biol. 5*, 1024–1037.
2. Kentner, D., and Sourjik, V. (2006) Spatial organization of the bacterial chemotaxis system. *Curr. Opin. Microbiol. 9*, 619–624.
3. Francis, N. R., Wolanin, P. M., Stock, J. B., Derosier, D. J., and Thomas, D. R. (2004) Three-dimensional structure and organization of a receptor/signaling complex. *Proc. Natl. Acad. Sci. U.S.A. 101*, 17480–17485.
4. Briegel, A., Ding, H. J., Li, Z., Werner, J., Gitai, Z., Dias, D. P., Jensen, R. B., and Jensen, G. J. (2008) Location and architecture of the *Caulobacter crescentus* chemoreceptor array. *Mol. Microbiol. 69*, 30–41.
5. Khursigara, C. M., Wu, X., Zhang, P., Lefman, J., and Subramaniam, S. (2008) Role of HAMP domains in chemotaxis signaling by bacterial chemoreceptors. *Proc. Natl. Acad. Sci. U.S.A. 105*, 16555–16560.
6. Khursigara, C. M., Wu, X., and Subramaniam, S. (2008) Chemoreceptors in *Caulobacter crescentus*: trimers of receptor dimers in a partially ordered hexagonally packed array. *J. Bacteriol. 190*, 6805–6810.
7. Zhang, P., Khursigara, C. M., Hartnell, L. M., and Subramaniam, S. (2007) Direct visualization of *Escherichia coli* chemotaxis receptor arrays using cryo-electron microscopy. *Proc. Natl. Acad. Sci. U.S.A. 104*, 3777–3781.
8. Zhang, P., Weis, R. M., Peters, P. J., and Subramaniam, S. (2007) Electron tomography of bacterial chemotaxis receptor assemblies. *Methods Cell Biol. 79*, 373–384.
9. Lefman, J., Zhang, P., Hirai, T., Weis, R. M., Juliani, J., Bliss, D., Kessel, M., Bos, E., Peters, P. J., and Subramaniam, S. (2004) Three-dimensional electron microscopic imaging of membrane invaginations in *Escherichia coli* overproducing the chemotaxis receptor Tsr. *J. Bacteriol. 186*, 5052–5061.
10. Wolanin, P. M., Baker, M. D., Francis, N. R., Thomas, D. R., DeRosier, D. J., and Stock, J. B. (2006) Self-assembly of receptor/

signaling complexes in bacterial chemotaxis. *Proc. Natl. Acad. Sci. U.S.A. 103*, 14313–14318.
11. Weis, R. M., Hirai, T., Chalah, A., Kessel, M., Peters, P. J., and Subramaniam, S. (2003) Electron microscopic analysis of membrane assemblies formed by the bacterial chemotaxis receptor Tsr. *J. Bacteriol. 185*, 3636–3643.
12. Bass, R. B., Butler, S. L., Chervitz, S. A., Gloor, S. L., and Falke, J. J. (2007) Use of site-directed cysteine and disulfide chemistry to probe protein structure and dynamics: applications to soluble and transmembrane receptors of bacterial chemotaxis. *Methods Enzymol. 423*, 25–51.
13. Swain, K. E., and Falke, J. J. (2007) Structure of the conserved HAMP domain in an intact, membrane-bound chemoreceptor: a disulfide mapping study. *Biochemistry 46*, 13684–13695.
14. Studdert, C. A., and Parkinson, J. S. (2005) Insights into the organization and dynamics of bacterial chemoreceptor clusters through in vivo crosslinking studies. *Proc. Natl. Acad. Sci. U.S.A. 102*, 15623–15628.
15. Studdert, C. A., and Parkinson, J. S. (2004) Crosslinking snapshots of bacterial chemoreceptor squads. *Proc. Natl. Acad. Sci. U.S.A. 101*, 2117–2122.
16. Milburn, M. V., Prive, G. G., Milligan, D. L., Scott, W. G., Yeh, J., Jancarik, J., Koshland, D. E., Jr., and Kim, S. H. (1991) Three-dimensional structures of the ligand-binding domain of the bacterial aspartate receptor with and without a ligand. *Science 254*, 1342–1347.
17. Kim, K. K., Yokota, H., and Kim, S. H. (1999) Four-helical-bundle structure of the cytoplasmic domain of a serine chemotaxis receptor. *Nature 400*, 787–792.
18. Hulko, M., Berndt, F., Gruber, M., Linder, J. U., Truffault, V., Schultz, A., Martin, J., Schultz, J. E., Lupas, A. N., and Coles, M. (2006) The HAMP domain structure implies helix rotation in transmembrane signaling. *Cell 126*, 929–940.
19. Park, S. Y., Borbat, P. P., Gonzalez-Bonet, G., Bhatnagar, J., Pollard, A. M., Freed, J. H., Bilwes, A. M., and Crane, B. R. (2006) Reconstruction of the chemotaxis receptor-kinase assembly. *Nat. Struct. Mol. Biol. 13*, 400–407.
20. Pollard, A. M., Bilwes, A. M., and Crane, B. R. (2009) The structure of a soluble chemoreceptor suggests a mechanism for propagating conformational signals. *Biochemistry 48*, 1936–1944.
21. Kim, S. H., Wang, W., and Kim, K. K. (2002) Dynamic and clustering model of bacterial chemotaxis receptors: structural basis for signaling and high sensitivity. *Proc. Natl. Acad. Sci. U.S.A. 99*, 11611–11615.
22. Shimizu, T. S., Le Novere, N., Levin, M. D., Beavil, A. J., Sutton, B. J., and Bray, D. (2000) Molecular model of a lattice of signalling proteins involved in bacterial chemotaxis. *Nat. Cell Biol. 2*, 792–796.
23. Briegel, A., Ortega, D. R., Tocheva, E. I., Wuichet, K., Li, Z., Chen, S., Muller, A., Iancu, C. V., Murphy, G. E., Dobro, M. J., Zhulin, I. B., and Jensen, G. J. (2009) Universal architecture of bacterial chemoreceptor arrays. *Proc. Natl. Acad. Sci. U.S.A. 106*, 17181–17186.
24. Dunten, P., and Koshland, D. E., Jr. (1991) Tuning the responsiveness of a sensory receptor via covalent modification. *J. Biol. Chem. 266*, 1491–1496.
25. Li, J., Li, G., and Weis, R. M. (1997) The serine chemoreceptor from *Escherichia coli* is methylated through an inter-dimer process. *Biochemistry 36*, 11851–11857.
26. Shrout, A. L., Montefusco, D. J., and Weis, R. M. (2003) Template-directed assembly of receptor signaling complexes. *Biochemistry 42*, 13379–13385.
27. Murphy, O. J., III, Kovacs, F. A., Sicard, E. L., and Thompson, L. K. (2001) Site-directed solid-state NMR measurement of a ligand-induced conformational change in the serine bacterial chemoreceptor. *Biochemistry 40*, 1358–1366.
28. Kott, L., Braswell, E. H., Shrout, A. L., and Weis, R. M. (2004) Distributed subunit interactions in CheA contribute to dimer stability: a sedimentation equilibrium study. *Biochim. Biophys. Acta 1696*, 131–140.
29. Sanders, D. A., Gillece-Castro, B. L., Stock, A. M., Burlingame, A. L., and Koshland, D. E., Jr. (1989) Identification of the site of phosphorylation of the chemotaxis response regulator protein, CheY. *J. Biol. Chem. 264*, 21770–21778.
30. Montefusco, D. J., Shrout, A. L., Besschetnova, T. Y., and Weis, R. M. (2007) Formation and activity of template-assembled receptor signaling complexes. *Langmuir 23*, 3280–3289.
31. Gegner, J. A., Graham, D. R., Roth, A. F., and Dahlquist, F. W. (1992) Assembly of an MCP receptor, CheW, and kinase CheA complex in the bacterial chemotaxis signal transduction pathway. *Cell 70*, 975–982.
32. Asinas, A. E., and Weis, R. M. (2006) Competitive and cooperative interactions in receptor signaling complexes. *J. Biol. Chem. 281*, 30512–30523.
33. Scopes, R. K. (1994) Protein purification: priciples and practice, 3rd ed., Springer-Verlag, New York.
34. Pikal-Cleland, K. A., Rodriguez-Hornedo, N., Amidon, G. L., and Carpenter, J. F. (2000) Protein denaturation during freezing and thawing in phosphate buffer systems: monomeric and tetrameric beta-galactosidase. *Arch. Biochem. Biophys. 384*, 398–406.
35. Weldeghiorghis, T. K., and Schaefer, J. (2003) Compensating for pulse imperfections in REDOR. *J. Magn. Reson. 165*, 230–236.
36. Bak, M., Schultz, R., Vosegaard, T., and Nielsen, N. C. (2002) Specification and visualization of anisotropic interaction tensors in polypeptides and numerical simulations in biological solid-state NMR. *J. Magn. Reson. 154*, 28–45.
37. Bak, M., Rasmussen, J. T., and Nielsen, N. C. (2000) SIMPSON: a general simulation program for solid-state NMR spectroscopy. *J. Magn. Reson. 147*, 296–330.
38. Bass, R. B., and Falke, J. J. (1998) Detection of a conserved alpha-helix in the kinase-docking region of the aspartate receptor by cysteine and disulfide scanning. *J. Biol. Chem. 273*, 25006–25014.
39. Bass, R. B., and Falke, J. J. (1999) The aspartate receptor cytoplasmic domain: in situ chemical analysis of structure, mechanism and dynamics. *Structure 7*, 829–840.
40. Graesser, D. T., Wylie, B. J., Nieuwkoop, A. J., Franks, W. T., and Rienstra, C. M. (2007) Long-range $^{19}F$-$^{15}N$ distance measurements in highly-$^{13}C$, $^{15}N$-enriched solid proteins with 19F-dephased REDOR shift (FRESH) spectroscopy. *Magn. Reson. Chem. 45* (Suppl. 1), S129–S134.
41. Lin, L. N., Li, J., Brandts, J. F., and Weis, R. M. (1994) The serine receptor of bacterial chemotaxis exhibits half-site saturation for serine binding. *Biochemistry 33*, 6564–6570.
42. Li, G., and Weis, R. M. (2000) Covalent modification regulates ligand binding to receptor complexes in the chemosensory system of *Escherichia coli*. *Cell 100*, 357–365.
43. Antommattei, F. M., Munzner, J. B., and Weis, R. M. (2004) Ligand-specific activation of *Escherichia coli* chemoreceptor transmethylation. *J. Bacteriol. 186*, 7556–7563.
44. Falke, J. J., Dernburg, A. F., Sternberg, D. A., Zalkin, N., Milligan, D. L., and Koshland, D. E., Jr. (1988) Structure of a bacterial sensory receptor. A site-directed sulfhydryl study. *J. Biol. Chem. 263*, 14850–14858.
45. Rozovsky, S., and McDermott, A. E. (2001) The time scale of the catalytic loop motion in triosephosphate isomerase. *J. Mol. Biol. 310*, 259–270.
46. Frericks, H. L., Zhou, D. H., Yap, L. L., Gennis, R. B., and Rienstra, C. M. (2006) Magic-angle spinning solid-state NMR of a 144 kDa membrane protein complex: *E. coli* cytochrome $bo_3$ oxidase. *J. Biomol. NMR 36*, 55–71.
47. Hu, K. N., Havlin, R. H., Yau, W. M., and Tycko, R. (2009) Quantitative determination of site-specific conformational distributions in an unfolded protein by solid-state nuclear magnetic resonance, *J. Mol. Biol. 239*, 1055−1073.
48. Weliky, D. P., Bennett, A. E., Zvi, A., Anglister, J., Steinbach, P. J., and Tycko, R. (1999) Solid-state NMR evidence for an antibody-dependent conformation of the V3 loop of HIV-1 gp120. *Nat. Struct. Biol. 6*, 141–145.
49. Sharpe, S., Kessler, N., Anglister, J. A., Yau, W. M., and Tycko, R. (2004) Solid-state NMR yields structural constraints on the V3 loop from HIV-1 Gp120 bound to the 447−52D antibody Fv fragment. *J. Am. Chem. Soc. 126*, 4979–4990.
50. Sharpe, S., Yau, W. M., and Tycko, R. (2006) Structure and dynamics of the HIV-1 Vpu transmembrane domain revealed by solid-state NMR with magic-angle spinning. *Biochemistry 45*, 918–933.
51. Ames, P., and Parkinson, J. S. (2006) Conformational suppression of inter-receptor signaling defects. *Proc. Natl. Acad. Sci. U.S.A. 103*, 9292–9297.
52. Ames, P., Studdert, C. A., Reiser, R. H., and Parkinson, J. S. (2002) Collaborative signaling by mixed chemoreceptor teams in *Escherichia coli*. *Proc. Natl. Acad. Sci. U.S.A. 99*, 7060–7065.
53. Liu, J. D., and Parkinson, J. S. (1991) Genetic evidence for interaction between the CheW and Tsr proteins during chemoreceptor signaling by *Escherichia coli*. *J. Bacteriol. 173*, 4941–4951.
54. Pooransingh-Margolis, N., Renirie, R., Hasan, Z., Wever, R., Vega, A. J., and Polenova, T. (2006) $^{51}V$ solid-state magic angle spinning NMR spectroscopy of vanadium chloroperoxidase. *J. Am. Chem. Soc. 128*, 5190–5208.
55. Sun, S. J., Siglin, A., Williams, J. C., and Polenova, T. (2009) Solid-state and solution NMR studies of the CAP-Gly domain of mammalian dynactin and its interaction with microtubules. *J. Am. Chem. Soc. 131*, 10113–10126.
56. Seidel, K., Andronesi, O. C., Krebs, J., Griesinger, C., Young, H. S., Becker, S., and Baldus, M. (2008) Structural characterization of $Ca^{2+}$-ATPase-bound phospholarnban in lipid bilayers by solid-state nuclear magnetic resonance (NMR) spectroscopy. *Biochemistry 47*, 4369–4376.